Microscopic optical anisotropy of exciton-polaritons in a GaAs-based semiconductor microcavity

L. F. Lastras-Martínez,* E. Cerda-Méndez, N. Ulloa-Castillo,† R. Herrera-Jasso, L. E. Rodríguez-Tapia, O. Ruiz-Cigarrillo, and R. Castro-García‡

Instituto de Investigación en Comunicación Optica, Universidad Autónoma de San Luis Potosí, Alvaro Obregón 64, 78000 San Luis Potosí, San Luis Potosí, México

K. Biermann and P. V. Santos§

Paul-Drude-Institut für Festkörperelektronik, Hausvogteiplatz 5-7, 10117 Berlin, Germany

(Received 9 May 2017; revised manuscript received 4 December 2017; published 18 December 2017)

Exciton-polaritons in semiconductor microcavities are ideal for the study of the exciton-light interaction and its dependence on light polarization. In this work, we report on the optical response and the dependence on polarization of a polariton microcavity using microreflectance anisotropy spectroscopy (μ-RAS) with a spatial resolution of $10.0 \times 10.0\ \mu m^2$. We have found that, in contrast to optical reflection, the μ-RAS spectra are quite inhomogeneous along the microcavity surface. We demonstrate the existence of microscopic local domains with differences in optical anisotropy of up to 20% within 100 μm. These variations are independent of the detuning between the optical and excitonic resonances, which in our sample is close to 0 meV. The μ-RAS line shape can be understood by using a model based on the anisotropic strain fields induced at the interfaces of the microcavity. The model agrees quite well with the experimental results and allows us to quantify the split of the energy levels of the exciton-polariton branches induced by the local break of symmetry at the microcavity interfaces.

DOI: 10.1103/PhysRevB.96.235306

I. INTRODUCTION

The strong coupling of light and matter in semiconductor microcavities (MCs) has been the subject of intense study in the last two decades [1–3]. In MCs, light-matter quasiparticles called exciton-polaritons form by the quantum superposition of the photons and excitons confined in the optical cavity and in quantum wells (QWs) embedded in it, respectively. Fascinating phenomena such as quantum condensation [2,4,5], superfluidity [6], and formation of solitons with polaritons [7,8] have been demonstrated, opening a new venue for novel solid-state devices. Also, rich phenomena associated with the light polarization dependence of the polariton wave function have been reported [9].

A planar MC consists of two distributed Bragg reflectors (DBRs) surrounding a spacer layer that forms the cavity and embeds the QWs. A DBR is composed of a pile of $\lambda/4n$ layers (λ is the photonic resonance wavelength and n is the refraction index of the material) with alternating refraction indices. Since in (Al,Ga)As-based MCs the contrast in n between the $\lambda/4n$ layers is low, around 20 (or more) layer pairs are needed to get the required high reflectivity (R > 99%) of the DBR. This means that each DBR is a very thick layers stack (>2 μm). Since the lattice mismatch among the (Al,Ga)As alloys is very low, it is possible to grow the DBRs with a very low density of dislocations. Despite the very good planar homogeneity of the layers that can be achieved, the asymmetry of the interfaces in the direction of growth may have effects that are difficult to assess using standard characterization techniques such as reflectance or photoluminescence.

The reflectance anisotropy spectroscopy technique at microscopic scale (μ-RAS) has been shown to be a powerful optical technique for the characterization of surfaces and interfaces [10–12]. For example, using μ-RAS, it is possible to realize detailed spatial mappings of in-built strain at a buried interface [13], or to characterize surface defects [11]. The technique is noninvasive and can be used in air or under vacuum conditions. In contrast to conventional RAS setups [14], our μ-RAS spectrometer uses a charge-coupled device (CCD) camera as a light detector, which allows us to record RAS spectra from a region of $2.5 \times 2.5\ \mu m^2$ of sample under study [11]. The μ-RAS technique can thus be used to study the optical anisotropy properties of the light-matter coupling in the MC with spatial resolution.

In this paper we use μ-RAS to reveal microscopic defects in a (Al,Ga)As MC grown on GaAs (001) substrate. By measuring the difference in the reflectivity of light with two perpendicular polarizations, we map the difference in optical response with a spatial resolution of up to 10 μm. In contrast to optical reflection, which is quite homogeneous, μ-RAS spectra show significant variations, even within a region of 500 μm. By using a simple model, we fit the line shape of the measured spectra and find that it can be explained by energy splittings as large as 0.6 meV induced by a break of symmetry of the lower (LPB) and upper (UPB) polariton branches due to interfacial asymmetries. This work opens the possibility of characterization of a MC at a new level, allowing us, for example, to easily measure engineered strain-induced defects or patterns, which may be used to achieve novel functionalities such as polarization-dependent gain.

The paper is organized as follows: In the second section we give a description of the μ-RAS spectrometer and a description of the characterized MCs. The experimental results are presented in the third section. In the fourth section we

*lflm@cactus.iico.uaslp.mx

†Also at Paul-Drude-Institut für Festkörperelektronik, Hausvogteiplatz 5-7, 10117 Berlin, Germany.

‡Also at Universidad Autónoma de San Luis Potosí - CONACyT.

§santos@pdi-berlin.de

introduce the model used for the interpretation of the spectra discussed in the fifth section. Finally, Sec. VI summarizes the main conclusions of the work.

II. EXPERIMENTAL SETUP AND SAMPLE DESCRIPTION

In the experimental setup, the light from a 100 W tungsten lamp is filtered through a monochromator of focal length of 0.5 m. The monocromatic output light is collimated (beam diameter of 5.0 mm) and directed to the sample [(001) surface] through a linear polarizer prism and a photoelastic modulator (PEM) device *in tandem*. The linear polarizer axis is parallel to the [110] direction of the sample. When the PEM is turned on, it periodically modulates the beam between two linear polarizations parallel to the [110] and [1$\bar{1}$0] sample directions at a frequency of 100 kHz, producing a vanishing time-averaged polarization. When it is off, the polarization fixed by the prism is conserved. The light reflected from the sample, which is enclosed in an optical cryostat, is then focused on a 512×512 pixel^2 CCD camera. The μ-RAS signal is obtained by subtracting an image taken with polarized light (PEM off) from one taken with (effectively) unpolarized light (PEM on), divided by the image obtained from their average. Images were recorded in the wavelength range from 760 nm (1.62 eV) to 785 nm (1.58 eV) with steps of 0.1 nm. The acquisition time of each image was 300 ms and the angle of incidence of the collimated beam $\approx 4.0^\circ$. The setup thus measures the difference in reflectance between [110] and [1$\bar{1}$0] polarization states of the (001) GaAs MC. A spatial map (spatial resolution of 10.0 μm) of the RAS of the sample is obtained by averaging the spectral information of four adjacent camera pixels. A detailed description of the spectrometer can be found in Ref [11].

The sample studied is a MC with a quality factor $Q > 1000$ grown on a GaAs (001) substrate. The structure consists of an AlAs cavity with optical thickness of $\lambda/2$ containing three groups of four GaAs(7 nm)/AlAs(5 nm) QWs. Each QWs group is located at the antinodes of the confined optical mode. The lower and upper DBRs consist of 25 and 20 pairs, respectively, of $Al_{0.15}Ga_{0.85}As$ and $Al_{0.8}Ga_{0.2}As$ $\lambda/4$ layers. A detailed description of the growth procedure can be found in Ref. [15].

III. EXPERIMENTAL RESULTS

Figure 1 shows microreflectance (μ-R) spectra of the MC measured at different positions along the straight line on the sample surface shown in Fig. 2(B). The measurements were carried out at T = 20 K. Each spectrum is taken from a surface area of 10×10 μm^2. The distance labels for each spectrum (indicated next to each curve) are relative to the position of spectrum (a) [see Fig. 2(B)]. The spectra comprise two dips centered around $E_L = 1.59$ eV and $E_U = 1.6025$ eV that correspond to the lower polariton branch (LPB) and upper polariton branch (UPB), respectively. The energy difference $V_R = 12.5$ meV corresponds to the Rabi energy splitting. Although it is possible to observe differences among the spectra, such as different relative amplitudes between the LPB and the UPB and small energy shifts, the μ-R line shapes remain very similar.

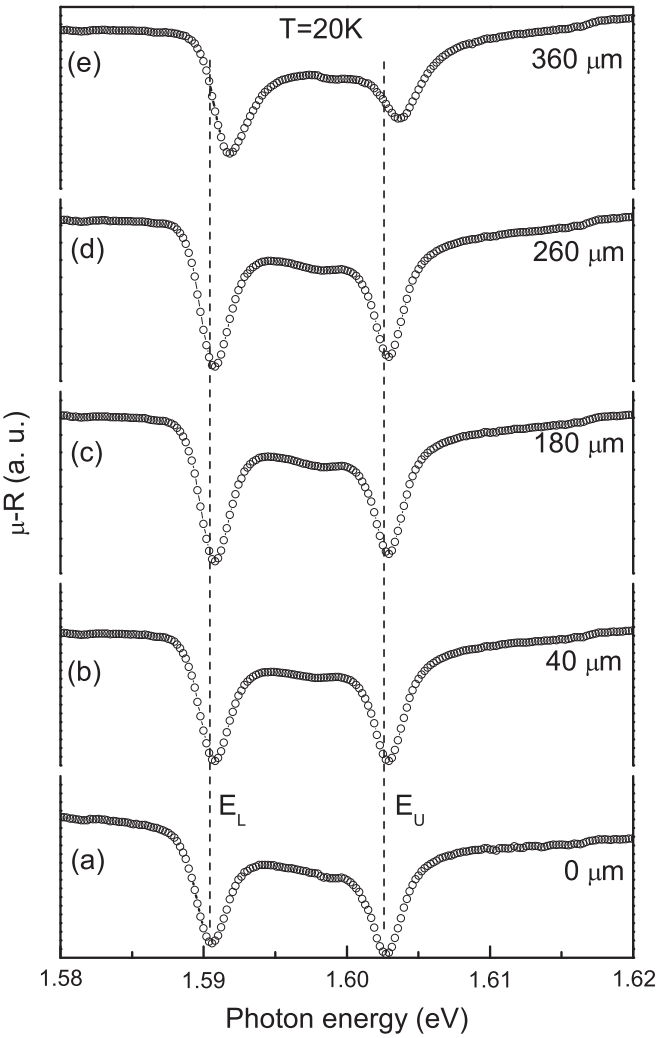

FIG. 1. Microreflectance spectra of the MC for different regions along a straight line at the sample surface. Each spectrum comes from a surface region of 10×10 μm^2. The distance between spectra relative to the spectrum (a) is indicated. Note that the line shapes of the microreflectance spectra of each region are practically the same along the surface. The energies E_L and E_U indicated by the dashed lines correspond to the energy positions of the LPB and UPB, respectively. The μ-R spectra are defined as the numerical addition of the reflectance spectra measured with the PEM turned on and the PEM turned off [11].

In contrast to the μ-R lineshapes, the μ-RAS spectra show marked differences [Fig. 2(A)]. For example, spectra (a) and (e) have comparable absolute RAS amplitudes but opposite signs, while the anisotropy becomes significantly reduced in spectra (b), (c), and (d). By scanning over a larger region along the surface, we found that the amplitudes of spectra (a) and (e) are the largest ones found on the surface. Consequently, these regions have the maximum possible anisotropy. The spatial dependence of the μ-RAS signal of the LPB is displayed in Fig. 2(B). The signal was estimated by taking the difference between the maximum and the minimum of the optical structure associated with the LPB. The horizontal arrows indicate the exact points at the scan line where the spectra of Figs. 1 and 2(A) were recorded.

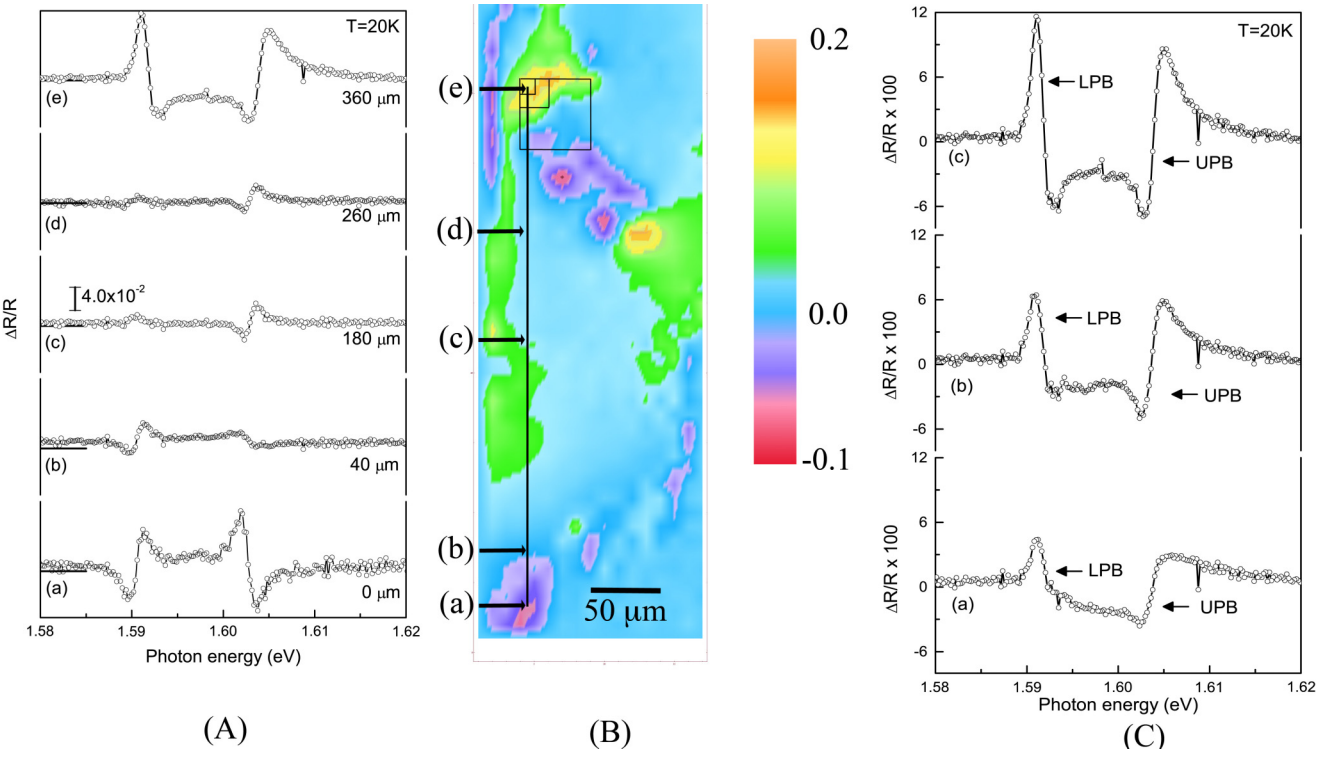

FIG. 2. (A) RAS spectra of the MC at different positions along the straight line at the surface indicated by the horizontal arrows in (B). Each spectrum comes from a surface region of $10 \times 10\ \mu m^2$. The distance between spectra relative to the spectrum (a) is indicated. Note that the line shapes of the reflectance difference anisotropy spectra vary considerably with position. (B) RAS map of the MC. The map was obtained by taking the difference between the maximum and the minimum of the $\Delta R/R$ signal at the energy range of the lower polariton. The resolution is $10 \times 10\ \mu m^2$. (C) RAS obtained by numerically averaging μ-RAS spectra in regions of (a) $50 \times 50\ \mu m^2$, (b) $20 \times 20\ \mu m^2$, and (c) $10 \times 10\ \mu m^2$. Each region is indicated by the squares in the map of Fig. 2(B).

Linear dichroism in GaAs microcavities has been measured by transmission in Ref. [16]. In that case, a light spot of 50 μm of diameter was used. We point out here that with this resolution it is not possible to resolve the μ-RAS signal in detail. This is evident from Fig. 2(C), where the spectra taken from the regions marked by the squares in Fig. 2(B) are shown. The spectrum (a) of Fig. 2(C) is equivalent to the one reported in the literature [16], where the signal appears as a combination of a derivative and a peak-like line shape [16]. In our case, by using a resolution of $10 \times 10\ \mu m^2$, we show that the μ-RAS spectra is instead associated with a derivative-like line shape only.

From the evolution of the μ-RAS spectra in Fig. 2(A), we draw the following conclusions. (i) Considering that spectra (a) and (e) have the maximum amplitudes, they can be taken as the "base" line shapes with which the spectrum of any other point of the sample can be reconstructed by a linear combination of them. Note, however, that the spectra are rigidly shifted in energy from one region to another, which must be taken into account when calculating the linear combination. (ii) The smaller μ-RAS amplitudes for the spectra other than (a) and (e) can be understood by considering that they stem from a region containing domains with both, (a) and (e)-like anisotropies. We show in the next sections that anisotropies of opposite signs arise from differences between the interfaces of the MC and the QWs.

IV. MODEL

The energies of the UPB (E_U) and LPB (E_L) are given by

$$E_{U,L} = \underbrace{\frac{\omega_c + \omega_{ex}}{2}\hbar}_{E_\alpha} \pm \underbrace{\frac{1}{2}\sqrt{\Delta^2 + V_R^2}}_{E_\beta}, \qquad (1)$$

where the upper and lower signs correspond to UPB and LPB, respectively. The symbols ω_c and ω_{ex} are the frequencies of the uncoupled optical cavity mode and the exciton, respectively. V_R is the Rabi coupling and Δ is the cavity detuning, defined as $\Delta = \hbar(\omega_c - \omega_{ex})$. By symmetry, the parameters V_R and Δ are independent of the light polarization for a (001) GaAs MC, so that the energy given by Eq. (1) is expected to be isotropic.

Different sources of anisotropies have been suggested for polariton MCs [16,17]. Polaritons are a combination of an excitonic and a photonic eigenstate. In the bulk of a zinc blende semiconductors, the heavy hole ($\psi^{hh}_{\pm 3/2}$) and light hole ($\psi^{lh}_{\pm 1/2}$) states are degenerate. These states split inside a QW, where the lowest excitonic state is formed by the heavy hole and the conduction ($\psi^{c}_{\pm 1/2}$) band states. Due to symmetry, the reflectance for light polarization along [110] and [1$\bar{1}$0] directions is expected to be the same for MCs on (001) GaAs. An anisotropy is expected if the heavy and light states are mixed as a result of an asymmetry of the QWs or the presence of residual strain and/or a built-in electric field. The mixture

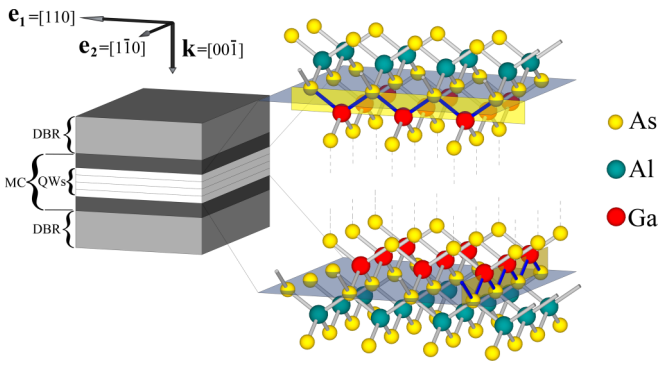

FIG. 3. Structure of the sample used in this work. The three groups of the four GaAs(7 nm)/AlAs(5 nm) QWs are indicated by the lines within the MC region. At each interface of the MC (indicated by the gray shaded planes) an anisotropy of opposite signs is expected. We illustrate this fact in the right part of the figure. The upper and lower bounds in the arsenic atoms at the interfaces of the MC are rotated by 90° with respect to the surface of the sample. Upper and lower bounds at each interface are highlighted in blue and their orientations are indicated by yellow planes.

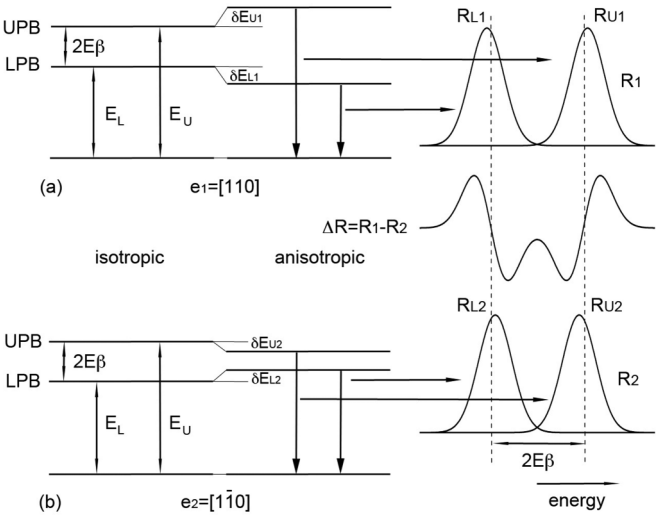

FIG. 4. Energy bands of the polaritons. Valence bands are split due to the break of symmetry within the quantum well leading to an anisotropy. Due to the anisotropy a polarization dependence of the splitting is predicted. For polarization along the [110] direction the splitting is increased while for [0$\bar{1}$1] direction the splitting is decreased. In the right part of the figure, we show the line shape of the simulated reflectance for each polarization. We also show the RAS signal obtained by the difference of spectra along [110] minus spectra along [1$\bar{1}$0]. Note that the RAS line shape resembles the first derivative of energy, and the contributions of the upper and lower polaritons to the RAS spectra are reversed in sign.

of the $(\psi^{hh}_{\pm 3/2})$ and $(\psi^{lh}_{\pm 1/2})$ states leads to a dependence on polarization of the interband matrix element of the optical transitions and thus to different Rabi couplings V_R for [110] and [1$\bar{1}$0] linear polarizations. Additionally, if the Bragg reflectors or the cavity are slightly birefringent, the frequency ω_c of the uncoupled cavity mode and, thus, the cavity detuning Δ will depend on optical polarization [16,17].

A further source of anisotropy is associated with the interfaces, where the zinc blende symmetry is locally broken. Figure 3 illustrates the atomic configuration of the interfaces (indicated by the gray shaded planes) of the QWs embedded in the MC. At the upper interface, each As interface atom is bounded to Al and to Ga atoms from the upper and lower layers, respectively. The configuration of the bonds is such that the interface has only a twofold rotation axis and different optical responses for polarizations along the [110] and [1$\bar{1}$0] directions. The same applies to the lower interface, but in this case the anisotropy is reversed in sign due to the 90° rotation of the bonds. The bonds at the interfaces are highlighted in blue and their orientations are indicated by the yellow planes. If the two interfaces are equivalent, their anisotropy contributions will cancel each other. However, the interfaces are in general not equivalent. For instance, the roughness and diffusion gradients of As or vacancies introduced during the growth process are in general different for the upper and lower interfaces of each layer. It is known that As vacancies and their gradient distribution through the QW generates an anisotropic strain field at the interfaces [18]. The relative orientation of these fields at the upper and lower interfaces of a QW is rotated by 90° around the [001] axis, thus leading to optical anisotropies with opposite signs. The anisotropic strain field is expected to modify the values of V_R and Δ, leading to a dependence of these parameters on the light polarization.

Figure 4 shows the energy states involved in the formation of a polariton for light polarization along the (a) $e_1 = [110]$ and (b) $e_2 = [1\bar{1}0]$ directions. In the isotropic case the transition energies E_L and E_U are the same for both polarizations. For the anisotropic case, in contrast, these energy levels depend on polarization. For instance, Fig. 4 illustrates a particular situation where the Rabi splitting increases for (a) and decreases for (b). The corresponding R and RAS are displayed on the right panels. The reflectance for each polarization is defined as $R_1 = R_{L1} + R_{U1}$ and $R_2 = R_{L2} + R_{U2}$, where $R_{L1(2)}$ and $R_{U1(2)}$ are the contributions to the reflectance spectra of each polariton branch. In the isotropic case $R_L = R_{L1} = R_{L2}$ and $R_U = R_{U1} = R_{U2}$. In the anisotropic case illustrated in Fig. 4, for light polarization parallel to [110], the energy difference between R_{L1} and R_{U1} increases, whereas for [1$\bar{1}$0] polarization the energy difference between R_{L2} and R_{U2} decreases. Considering that the RAS signal is proportional to $\Delta R = R_1 - R_2$, one obtains a first-derivative-like shape as is illustrated in the figure. Note, in addition, that the RAS signal has different signs for the upper and lower polaritons.

According to the discussion of the previous paragraphs, the anisotropies induced by energy splittings of the polariton bands can be written as an energy derivative whose form is given by,

$$\frac{\Delta R}{R} = \frac{1}{R_L}\frac{dR_L}{dE}\delta E_L + \frac{1}{R_U}\frac{dR_U}{dE}\delta E_U, \qquad (2)$$

where $\delta E_L = \delta E_{L1} + \delta E_{L2}$ and $\delta E_U = \delta E_{U1} + \delta E_{U2}$ are the energy shifts between [110] and [1$\bar{1}$0] polarizations of the LPB and UPB. As we mentioned previously, R_L and R_U are the measured contributions to the reflectance spectra of each polariton.

The splittings δE_L and δE_U are functions of the anisotropy of ω_c and V_R. In the general case we obtain from differentiation

of Eq. (1) [16,17]

$$\delta E_{U,L} \approx \left(1 \pm \frac{\Delta}{2E_\beta}\right)\delta E_C \pm \frac{V_R}{4E_\beta}\delta V_R, \qquad (3)$$

where δE_C and δV_R are the anisotropies of the cavity and the Rabi coupling respectively. The upper and lower signs in the equation correspond to the UPB and the LPB respectively. Note that the energy splitting of the polaritons δE_U and δE_L are in general different. Only in the particular case where $\delta E_C = 0$ do the energy splittings for both polariton branches have the same absolute value. Thus, if the absolute values of the splittings δE_U and δE_L are similar, we can conclude that the μ-RAS signal is dominated by the anisotropy of the Rabi coupling δV_R, otherwise the anisotropies of the cavity δE_C must be considered. Equations (2) and (3) and the spectra of Fig. 1 will be used in the next section to fit and discuss the physical origin of the polariton anisotropies.

V. DISCUSSION

According to our model, the anisotropies can originate at any of the interfaces between the DBRs and the QWs. For a given a region within the MC, if both interfaces have an anisotropy of the same order of magnitude, the μ-RAS signal must have a small amplitude, since each interface contributes with opposite sign. Larger amplitudes of the μ-RAS signal indicate that the anisotropy of one of the interfaces is larger than the other.

The open circles in Figs. 5(a) and 5(b) display the basis (maximum RAS signal) spectra (a) and (e) of Fig. 2(A) together with the fits (solid lines) obtained by using Eq. (2). The fits were obtained independently by adjusting the energy of the LPB and UPB peaks using the contributions R_L and R_U from the R spectra of Fig. 1. For each contribution, we calculated numerically the first energy derivative. The derivatives were then divided by their corresponding reflectivities according to Eq. (2). Since the contributions to the μ-RAS spectra of the LPB and the UPB have opposite signs and different strengths, each contribution was multiplied by the adjustable parameter δE_L or δE_U, respectively. The values obtained for δE_L and δE_U are indicated in the figure.

We may then conclude the following. (i) For each spectrum, the line shape is first-derivative-like and has different sign contributions for the LPB and UPB in accordance with our model. (ii) Spectra (a) and (e) have different signs indicating that the anisotropy originates at different interfaces of the MC (see Fig. 3). (iii) The absolute values of the magnitudes of the splitting are almost the same for spectrum (a), indicating that the splittings are dominated by the anisotropy δV_R of the Rabi coupling. (iv) For the case of spectrum (b) the values of the splittings are different, indicating that not only is the anisotropy δV_R important but also the anisotropy associated with δE_C has measurable contributions.

To illustrate the composition of the line shape for spectra in different regions, we show in Fig. 5(c) the spectrum (d) of Fig. 2(A) and the fit (solid line) obtained by the superposition of spectra (a) and (b). The only adjustable parameter was a rigid energy shift, corresponding to the different hydrostatic

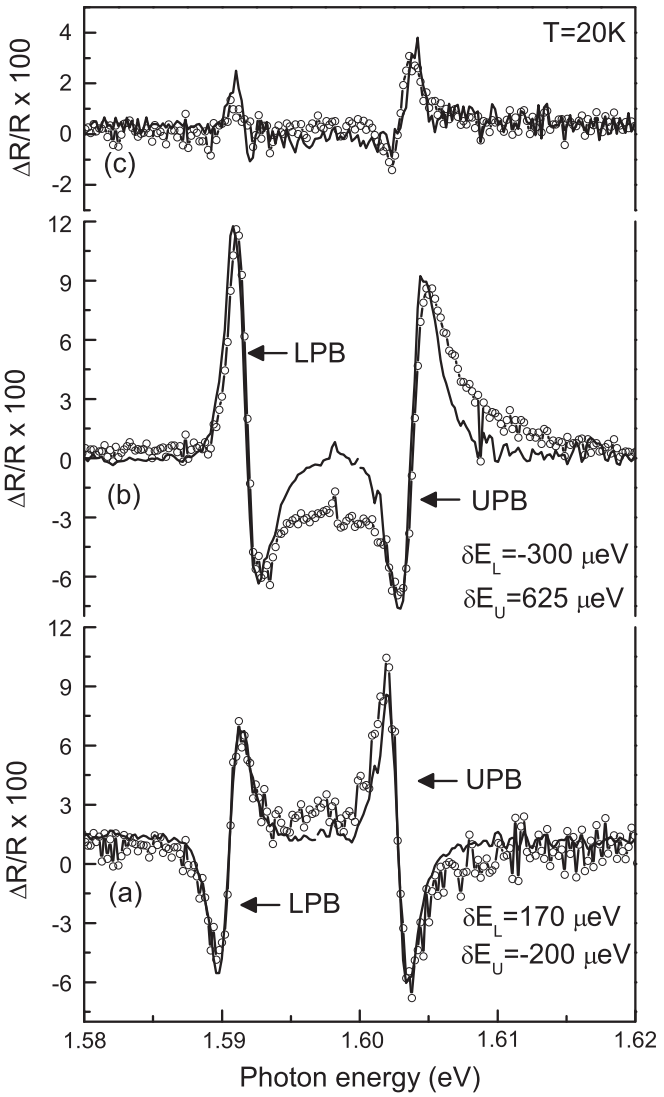

FIG. 5. (a) and (b) show the RAS spectra for the upper and lower polaritons. Spectra come from different areas of $10 \times 10\ \mu m^2$ separated by 320 μm. Note that the anisotropy signal changes sign indicating that it originates in different interfaces of the MC and QW. Solid lines are the spectra obtained by using the reflectance corresponding to spectra of Fig. 1 and Eq. (2). The values for δE_L and δE_U obtained by fitting the amplitudes of the spectra are indicated in the figure. Spectrum (c) shows the spectrum of Fig. 1(d). The solid line is the fit obtained by the superposition of the basic line shapes (a) and (b).

shift induced, for instance, by the strain at each interface. In this case, spectrum (a) was rigidly blue-shifted approximately 1.5 meV. The fits obtained in Fig. 5 are in excellent agreement with our model.

VI. CONCLUSIONS

μ-RAS spectroscopy is a powerful tool to measure the energy splitting of the lower and upper branches of MC polaritons. In particular μ-RAS allows sensing changes of energy splitting in the range of hundreds of μeV through the MC surface. The splitting is induced by the break of symmetry

of the exciton's wave function within the QW induced by the diffusion gradients of As or by defects or vacancies at the interfaces between the MC and the QW. We show that a spatial resolution of at least 10 μm is necessary to isolate the anisotropy associated to this break of symmetry at the interfaces.

ACKNOWLEDGMENTS

We would like to thank E. Ontiveros, F. Ramírez-Jacobo, L. E. Guevara-Macías, and J. Gonzalez-Fortuna for their skillful technical support. This work was supported by CONACyT (Grant No. 207713), DAAD (Grant No. 57064990), and Cátedras CONACyT (Grant No. 1577).

[1] D. Sanvitto and S. Kéna-Cohen, Nat. Mater. **15**, 1061 (2016).
[2] T. Byrnes, N. Y. Kim, and Y. Yamamoto, Nat. Phys. **10**, 803 (2014).
[3] A. Kavokin, Phys. Status Solidi B **247**, 1898 (2010).
[4] H. Deng, G. Weihs, C. Santori, J. Bloch, and Y. Yamamoto, Science **298**, 199 (2002).
[5] J. Kasprzak *et al.*, Nature (London) **443**, 409 (2006).
[6] A. Amo, J. Lefrère, C. Adrados, C. Ciuti, L. Carusotto, R. Houdré, E. Giacobino, and A. Bramati, Nat. Phys. **5**, 805 (2009).
[7] M. Sich, D. N. Krizhanovskii, M. S. Skolnick, A. V. Gorbach, R. Hartley, D. V. Skryabin, E. A. Cerda-Méndez, K. Biermann, R. Hey, and P. V. Santos, Nat. Photon. **6**, 50 (2012).
[8] E. A. Cerda-Méndez, D. Sarkar, D. N. Krizhanovskii, S. S. Gavrilov, K. Biermann, M. S. Skolnick, and P. V. Santos, Phys. Rev. Lett. **111**, 146401 (2013).
[9] I. A. Shelykh, A. V. Kavokin, Y. G. Rubo, T. C. H. Liew, and G. Malpuech, Semicond. Sci. Technol. **25**, 013001 (2010).
[10] W. Huang, Y. Liu, L. Zhu, X. Zheng, Y. Li, Q. Wu, Y. Wang, X. Wang, and Y. Chen, Opt. Express **24**, 15059 (2016).
[11] L. F. Lastras-Martínez, R. Castro-García, R. E. Balderas-Navarro, and A. Lastras-Martínez, Appl. Opt. **48**, 5713 (2009).
[12] E. A. Cerda-Méndez, R. E. Balderas-Navarro, A. Lastras-Martínez, L. F. Lastras-Martínez, A. Garnache, L. Cerutti, and A. Jouillé, J. Appl. Phys. **98**, 066107 (2005).
[13] L. F. Lastras-Martínez, R. Herrera-Jasso, N. A. Ulloa-Castillo, R. E. Balderas-Navarro, A. Lastras-Martínez, A. C. Lin, M. M. Fejer, and James S. Harris, J. Appl. Phys. **114**, 173504 (2013).
[14] D. E. Aspnes, Y. C. Chang, A. A. Studna, L. T. Florez, H. H. Farrell, and J. P. Harbison, Phys. Rev. Lett. **64**, 192 (1990).
[15] K. Biermann, E. A. Cerda-Méndez, M. Höricke, P. V. Santos, and R. Hey, J. Cryst. Growth **323**, 56 (2011).
[16] A. Brunetti, M. Vladimirova, S. Cronenberger, D. Scalbert, M. Nawrocki, and J. Bloch, Superlatt. Microstruct. **41**, 429 (2007).
[17] L. Klopotowski, M. D. Martín, A. Amo, L. Viña, I. A. Shelykh, M. M. Glazov, G. Malpuech, A. V. Kavokin, and R. André, Solid State Commun. **139**, 511 (2006).
[18] L. F. Lastras-Martínez, J. Ortega-Gallegos, R. E. Balderas-Navarro, J. M. Flores-Camacho, M. E. Chavira-Rodríguez, A. Lastras-Martínez, and M. Cardona, Phys. Status Solidi C **5**, 2591 (2008).